Int J Adv Manuf Technol (2001) 18:648–656

The International Journal of
Advanced
Manufacturing
Technology

Experimental and Analytical Balance Sheet in Turning Applications

O. Cahuc[1], P. Darnis[2], A. Gérard[1] and J.-L. Battaglia[3]

[1]Laboratoire de Mécanique Physique, UMR CNRS 5469, Université Bordeaux, Talence, France; [2]Laboratoire de Génie Mécanique, IUT A, Université Bordeaux, Talence, France; and [3]Laboratoire 'Energétique et Phénomènes de transfert, UMR CNRS 8508, Ecole Nationale Supérieure d'Arts et Métiers, Talence, France

In orthogonal, oblique, and 3D cutting, the assumption of point contact between the tool and the workpiece often results in the consideration of only the forces in the three principal directions. This paper disregards these assumptions and confirms the existence of moments around the three principal directions through measurements of the mechanical factors during a turning operation. The experimental method used reveals, through energy assessment, the contribution of the various components of the forces and moments to the power consumed during classical and hard turning operations.

By description of the various zones of contact chip/tool/workpiece, a new modelling of 3D cutting is presented. The analytical model developed takes into account the complete geometry of the tool and introduces a new concept in modelling, especially of the secondary shear zone.

A comparison between the power involved in the cutting process obtained with the model and with three other experimental devices confirms the relevance of 3D modelling, integrating the concept of moments at the tip of the tool. The energy balance equilibrium is then carried out correctly for the first time.

Keywords: Consumed power; Cutting process; Energy balance; Forces and moments; Thermal model; Three-dimensional model

1. Introduction

In machining by turning (Fig. 1), the removal of material from the workpiece as a chip arises from the cutting action between the tool insert and the cylindrical workpiece. Orthogonal cutting denotes a special configuration where the straight cutting edge of the tool is perpendicular to the direction of relative motion of the tool and workpiece. This special case has been extensively discussed in the literature [1–7] since it led to meaningful simplification in the thermomechanical modelling of such a process.

A 3D analytical model has been developed, taking into account the five principal zones observed in the cutting phenomena. This model uses previous results [1,3,6–10], in particular those concerning primary shearing. It proposes a new approach to the phenomena present in the secondary shearing zone. We consider that the secondary shearing zone at the interface between the tool and the chip can be compared to a micropolar medium [9]. It also integrates a modelling of the primary and secondary clearance zones and takes into account the edge and tool radius.

From the cutting conditions, tool geometry and thermomechanical characteristics of the material, and contact of the workpiece with the tool, the temperatures in the primary and secondary shearing zones are evaluated. Thus, the consumed power P_{mod} can be derived from the predicted forces and moments.

The paper is organised as follows. In Section 2, we study the cutting process phenomena in the five principal identified zones. These zones are completely described to explain the mechanical and thermal phenomena. Section 3 is devoted to

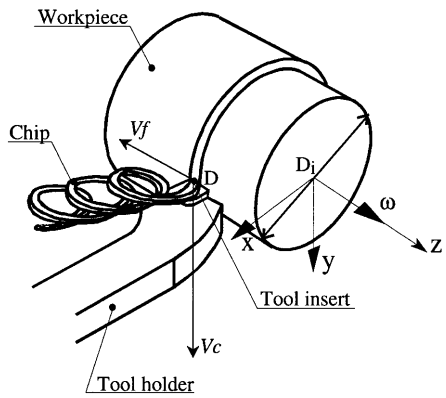

Fig. 1. The turning process description.

Correspondence and offprint requests to: O. Cahuc, Laboratoire de Mécanique Physique, UMR CNRS 5469, Université Bordeaux 1, 351 cours de la Libération, 33405 Talence Cedex, France. E-mail: o.cahuc@1mp.u-bordeaux.fr

the experimental technique used to determine the mechanical power consumed P_m and the mechanical power P_{prov} provided. The remainder of the paper is devoted to a comparison between P_{mod}, P_m, P_{prov}, and P_{th}.

2. Cutting Process Phenomenology

In machining and according to the cutting speed, selected trajectories and material hardness, a chip is created, from the workpiece at the contact between the workpiece and the tool (see Fig. 2).

In this case, machining is characterised by:

1. A relative movement (see Fig. 1) between the workpiece and the tool, resulting from the combination of the cutting movement (spindle speed ω in lathe machining) and feed motion (feed velocity V_f). These movements can be independent or combined (helicoid movement, for example).
2. Tool geometrical characteristics.
3. Cutting parameters for optimising the tool/material/machining combination for productivity.
4. Tool/workpiece/chip contact characteristics.

The main geometrical and kinematics parameters for turning are presented in Fig. 2. We limit our study to the case of homogeneous isotropic material with a Von Mises plastic threshold material in stationary conditions and we retain the plastic incompressibility assumption [11].

Thus, we consider that mechanical power provided by the turning machine and consumed during machining is converted into thermal power released during the material strain in the various principal zones. The cutting analyses at the tool–workpiece–chip interfaces show the existence of 4 zones according to Fig. 3.

1. The dead zone.
2. The primary shearing zone.
3. The secondary shearing zone.
4. The principal and secondary clearance zones.

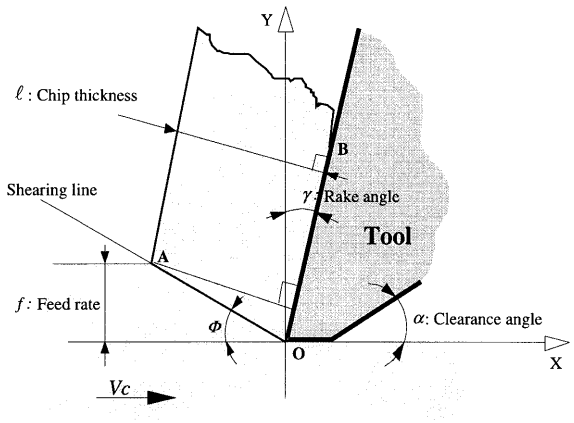

Fig. 2. Geometrical and kinematics parameters.

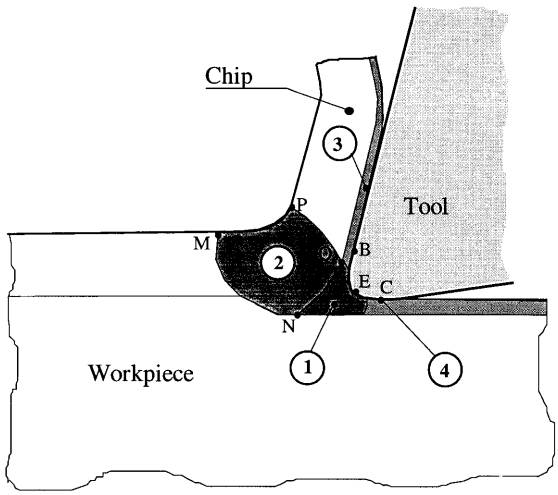

Fig. 3. The main zones characterizing cutting process.

2.1. Dead Zone

The material is divided into two parts. One part will constitute the new outer surface of the workpiece and the other will be the chip. Here, strain speed is so important that the reaction is exothermic and the matter is completely plasticised.

The matter is chased because tools always have a certain sharpness arising either from their natural geometrical form due to the sharpening or from the tool wear.

According to Albrecht [8], for the section *BE* (Fig. 3) the tool is chased whereas for the section EC the workpiece is chased.

2.2 Primary Shearing Zone

The primary shear zone coincides with *OA* (Fig. 2). The slip lines observed show that machined material is subjected to shear stress [12]. This is a slip plastic plane in which the chip is formed and characterised by its angle Φ and its thickness h_1 (Fig. 2).

The line *MN* (Fig. 3) denotes that the elastic limit is reached and line indicates the *PQ* end of the plastic flow which becomes solid flow. These phenomena generate a strain rate approximated by the ratio V_c/f (usually close to 10^5 s^{-1}). Moreover, shearing strains are usually higher than 50% involving a complete plasticisation of material.

The average strain speed $\dot{\bar{\gamma}}_{OA}$ is expressed by:

$$\dot{\bar{\gamma}}_{OA} = \frac{1}{h_1}\int_0^{h_1} \frac{\partial V_x}{\partial y}\,dy = \frac{V_c \sin(\gamma)}{h_1 \cos(\Phi - \gamma)} \tag{1}$$

where V_x is the x-axis component of the chip velocity vector (V_{chip}).

After integration, the average strain $\bar{\gamma}_{OA}$ is:

$$\bar{\gamma}_{OA} = \frac{\cos(\gamma)}{2\sin(\Phi)\cos(\Phi - \gamma)} \tag{2}$$

Thus, a particle which crosses the primary shearing zone (Fig. 4), is submitted to a strain and a strain speed defined by

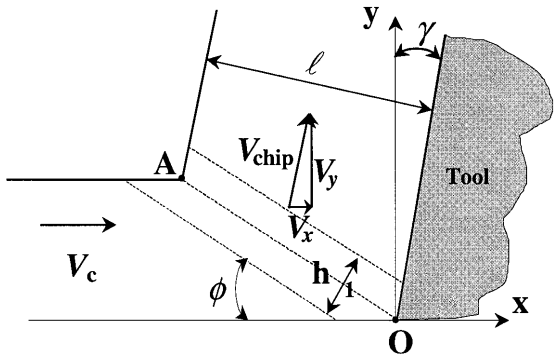

Fig. 4. The evolution of the velocities to the primary shearing interface.

ϵ_{OA} and $\dot{\epsilon}_{OA}$, respectively. Along the primary shearing line *OA*, the average strain speed is related to the generalised average strain speed by the relation:

$$\dot{\bar{\epsilon}}_{OA} = \frac{\dot{\gamma}_{OA}}{\sqrt{3}} \tag{3}$$

Some geometrical properties arising from this allow us to define $\dot{\bar{\epsilon}}_{OA}$ as in [13]:

$$\dot{\bar{\epsilon}}_{OA} = \frac{V_c \cos(\gamma)}{h_1 \sqrt{3} \cos(\Phi - \gamma)} \tag{4}$$

After integration, the generalised average strain $\bar{\epsilon}_{OA}$ along the primary shearing line *OA* can be expressed by:

$$\bar{\epsilon}_{OA} = \frac{\cos(\gamma)}{2\sqrt{3} \sin(\Phi) \cos(\Phi - \gamma)} \tag{5}$$

The equilibrium of a small element of matter ($\mathrm{d}n\mathrm{d}t \times 1$) of 1 unit width (see Fig. 5) is derived to estimate the hydrostatic distribution of pressure.

By projection on the *x*-axis, we obtain:

$$-\mathrm{d}p\mathrm{d}y + \frac{\mathrm{d}\sigma_{OA}}{\sqrt{3}}\,\mathrm{d}x = 0 \tag{6}$$

To integrate this differential equation we postulate that first the yield stress is influenced only a little by the temperature on *OA* ($\partial\sigma_{OA}/\partial\bar{\theta} = 0$) because variations in the temperature are low in this area and secondly the shearing plane is at the place of maximum shear ($\partial\sigma_{OA}/\partial\dot{\bar{\epsilon}} = 0$).

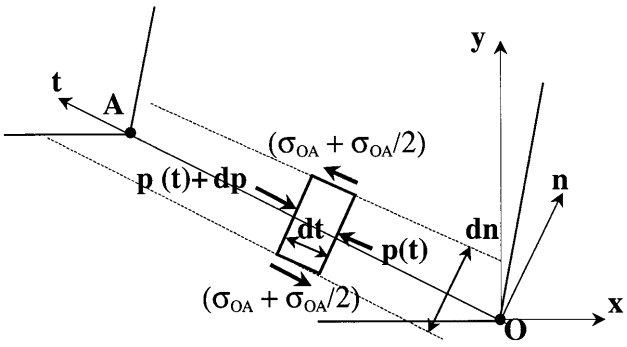

Fig. 5. Equilibrium stresses in primary shearing.

Therefore, the equilibrium stress equation can be expressed by [13]:

$$\frac{\partial\sigma_{OA}}{\partial\bar{\epsilon}}\frac{\mathrm{d}\bar{\epsilon}}{\mathrm{d}y} + \frac{\partial\sigma_{OA}\mathrm{d}\dot{\bar{\epsilon}}}{\partial\dot{\bar{\epsilon}}\,\mathrm{d}y} + \frac{\partial\sigma_{OA}}{\partial\bar{\theta}}\frac{\mathrm{d}\bar{\theta}}{\mathrm{d}y} = \sqrt{3}\,\frac{\mathrm{d}p(t)}{\mathrm{d}x} \tag{7}$$

where σ_{OA} denotes the flow stress in the primary shear and $p(t)$ is the hydrostatic pressure along *OA*.

The behaviour law allows the calculation of the partial derivative function of stress compared to the generalised strain.

The simplified differential equation can be expressed by:

$$\frac{\mathrm{d}p}{\mathrm{d}x} = \frac{2n\sigma_{OA}}{h_1\sqrt{3}} \tag{8}$$

Then, integration gives a distribution of linear and decreasing pressure along *OA:*

$$p(t) = \frac{2n\sigma_{OA}}{h_1\sqrt{3}}\,(t + H) \tag{9}$$

where constant *H* can be calculated from boundary conditions at point *A*.

From those considerations, one can assume a plane heat source located along *OA* [14] (see Fig. 6).

2.3 Secondary Shearing Zone

Kato et al. [15] found that this zone is a slip zone with intense friction between chip and tool. Microscopic analysis showed the existence of slip strips called shearing strips [12]. It is characterised by the following three principal parameters: its thickness $\delta \times l$, the chip thickness l and the tool–chip length of contact *OB* (Fig. 2).

In mechanical modelling, this zone is constituted as a boundary layer of thickness $\delta \times l$ ($\approx$0.001 mm) where δ is an estimated analytical coefficient. Then, we assume that the velocity profile varies linearly from 0 to V_{chip} in the second shear zone [13] (see Fig. 7).

In experiments, we observe the presence of an adherence zone between the tool and the chip in the secondary shearing. In this zone the chip velocity increases gradually from 0 to V_{chip} and is constant along the chip thickness. V_{chip} is then expressed by:

$$V_{chip} = V_c \frac{\sin\Phi}{\cos(\gamma - \Phi)} \tag{10}$$

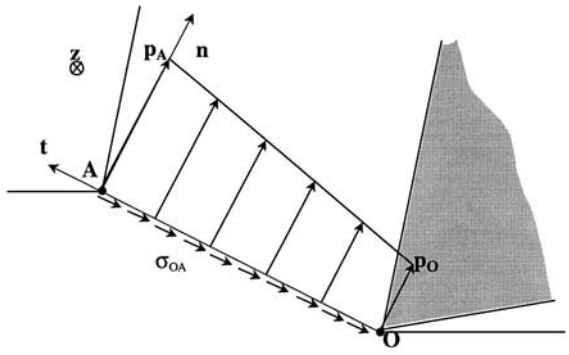

Fig. 6. Stress distribution along *OA*.

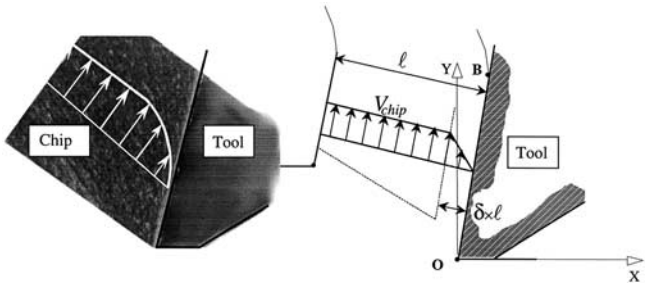

Fig. 7. Tool/chip interface micrography and modelling.

where γ and Φ are, respectively, the rake angle and the primary shear angle.

The energy balance method [16] allows us to define the average strain speed $\dot{\gamma}$at the plastic zone and rigid zone interface

$$\dot{\gamma}_{int} = \frac{1}{\delta \times l} \int_0^{\delta \times l} \frac{\partial V_x}{\partial y} \, dy = \frac{V_c \sin(\Phi)}{\delta \times l \cos(\Phi - \gamma_c)} \tag{11}$$

The generalised strain speed is taken equal to:

$$\dot{\epsilon}_{int} = \frac{\dot{\gamma}_{int}}{\sqrt{3}} \tag{12}$$

Generally, we assess that, in the secondary shear zone, strains are higher than 200 or 300% [10]. However, with these values, work hardening will be completed as soon as a strain of 100% is reached.

We suppose that in the *OC* zone (see Fig. 8), a pure couple is transmitted to the tool. It arises from a constant distribution **m** of stress torque [17,18] along the *OC* segment in the *Z*-direction. This assumption is based on the following: any material can be compared, according to the scale of observation, to a micropolar media [9]. We consider that the microstructure of a material can then transmit a stress torque [19]. Thus, the generalised strain is taken to be equal to unity in the behaviour law used for analytical modelling [13].

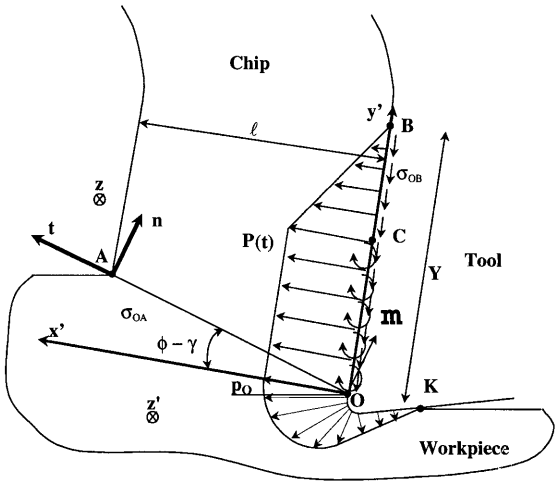

Fig. 8. Stress distribution along *KOB*.

The stress continuity in *O* allows the determination of σ_{OB} from σ_{OA}. Then, shearing is constant and equal to σ_{OB} on segment *OC*, and then decreases linearly from *C* to *B*.

$$\begin{cases} p(y') = p_0 & \forall y' \in [0,kY] \\ p(y') = \dfrac{p_0}{1-k} \dfrac{(Y - y')}{Y} & \forall y' \in [kY,Y] \end{cases} \tag{13}$$

where real *k* is computed for a minimal energy. Then, we find:

$$\begin{cases} \sigma_{OB}(y') = \sigma_{OB} & \forall y' \in [0,kY] \\ \sigma_{OB}(y') = \dfrac{\sigma_{OB}}{1-k} \dfrac{(Y - y')}{Y} & \forall y' \in [kY,Y] \end{cases} \tag{14}$$

2.4 Principal and Secondary Clearance Zones

In this zone, we consider that the tool penetrates the workpiece (zone *IJK* on Fig. 9) and the material remains in an elastic state [13]. The stress (from the hydrostatic pressure) and shear stresses at point *I* can be taken to be equal to that in *O*. Then, the pressure distribution along *IK* will be considered linear, becoming zero at *K* [20,21]. Moreover, we will suppose that this distribution is constant in the depth of cut direction. The length *L* is deduced from the hydrostatic pressure at *O* and the material elasticity modulus. Then, it is corrected to be a function of cutting speed V_c, feed velocity V_f and tool edge radius R_a [13]:

$$L = b \frac{p_0(1 + V_f)(-R_a + 1)}{E(1 + V_c)} \tag{15}$$

where p_0 is the constant pressure [20,21] along the normal direction at the cutting edge *IJ*, *E* is the material elasticity modulus and *b* is a constant deduced from an experimental result by using the Albrecht approach [8] in order to determine the force which acts on the clearance face (see Fig. 10). The length *L′* is calculated using geometrical considerations.

For the study of the 3D cut, similar considerations will allow, insofar as the cutting depth remains sufficiently large, us to show that almost the same thing occurs in the secondary clearance zone as in the primary clearance zone.

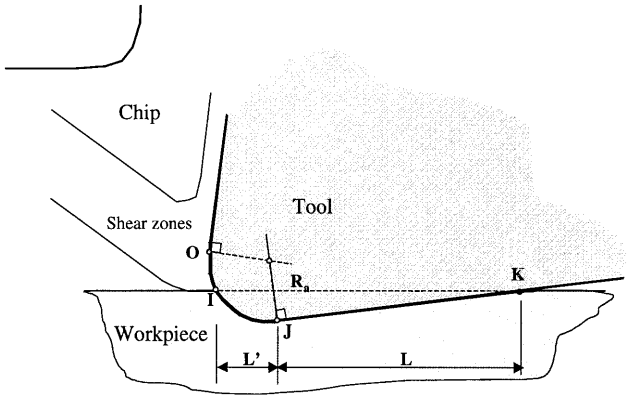

Fig. 9. Principal clearance zone model.

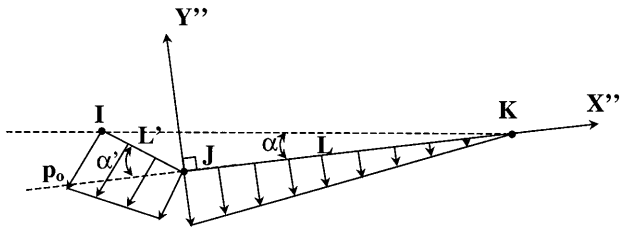

Fig. 10. Normal stress distribution along *IK*.

The normal and tangential forces will be found by integrating along the boundary zone *IK* giving the following triangular distributions:

$$p(s) = \frac{p_0(-s + L' - L)}{L' + L} \quad \forall s \in [0, L' + L] \tag{16}$$

$$\sigma(s) = \frac{\sigma_0(-s + L' - L}{L' + L} \quad \forall s \in [0, L' + L] \tag{17}$$

2.5 Behaviour Law

Cutting generates strain speeds (about V_c/f ratio), of about $10^5\ s^{-1}$ order. Strains are usually higher than 50%, thus work hardening of the material has a great influence. We will consider the relation of the yield stress with the temperature and work hardening coupling, through a behaviour law. The work hardening and viscosity are integrated as a power law and with a linear decrease with the temperature [13]:

$$\sigma = \epsilon^n \dot{\epsilon}^m (A - B\,\theta) \tag{18}$$

This linear approximation of the situation according to the temperature lets us estimate the source temperature. The integration of the differential equation then gives:

$$\overline{\theta}_1 = \overline{\theta}_0 - (1 - \beta_c)\frac{A^2}{B}\exp\left(\frac{-B\dot{\overline{\epsilon}}_1^m \overline{\epsilon}_1^{n+1}}{(n+1)\,\rho C_p}\right) \tag{19}$$

where β_c is the heat fraction given by experimental results [22].

For the secondary shearing zone, the thermal evolution law suggested by Oxley is used [6]. So, it is possible to evaluate the average temperature $\overline{\theta}_2$ at the tool–chip interface by considering that it is a linear function of the maximum heating $\Delta\theta_m$:

$$\overline{\theta}_2 = \overline{\theta}_1 + \Psi\Delta\theta_m \tag{20}$$

Thus, the knowledge of the phenomena present in the principal zones described above will allow us to estimate the mechanical power consumed P_{mod}.

3. Comparison Between Mechanical, Thermal and Electrical Powers Involved During Turning

3.1 Mechanical Power

In chip formation, very great energy is dissipated in small volumes of matter. Part of this energy is due to the presence of moments at the tool/workpiece interface. Then, the total mechanical power consumed by the cutting process is expressed by

$$P_m = F_{w/T}\, V_{D\in w} + M_{w/T}\,(D)\,\omega_w \tag{21}$$

where $F_{w/T} = \langle F_x\ F_y\ F_z \rangle$ and $M_{w/T}\ (D) = \langle M_x\ M_y\ M_z \rangle$ are the force and the moment vectors, respectively.

The standard ISO notation is used in order to represent components of forces and moments applied on the tool at point *D*, which is also the origin. All components will be expressed in the (*D*, *x*, *y*, *z*) reference axis, whatever the turning operation. According to whether one carries out face turning or longitudinal turning, *y*, $-z$, and *x* can be, respectively, the cutting speed V_c, the feed velocity V_f and the cutting depth a_p directions (Fig. 11). In order to measure the six components of forces and moments of the mechanical actions independently, an appropriate dynamometer has been developed [23].

In the case of longitudinal turning, the power can be expressed as:

$$P_m = F_y\, V_c + M_z\,(D)\,\omega + F_z V_f \tag{22}$$

We can see that three separate terms can be identified. The first is the cutting speed part $F_y V_c$ of the consumed power. The second is the moment part $M_z(D)\omega$. This term can represent, in certain cases, up to 50% of the total consumed power and must not be neglected [13]. The third term is the feed velocity part. This term is often negligible in comparison with the other two terms, as shown by experiments.

3.2 Thermal Power

The thermal power P_{th} dissipated during the turning process arises from the degradation of the mechanical power into heat in the neighbourhood of the cutting zone. Heat fluxes in the workpiece, the chip, and the tool are estimated from the resolution of the inverse heat conduction problems in these three components [2,24–31].

We assume a quasi-stationary condition. That means that the temperature distribution in the cutting domain soon becomes independent of time. This supposes that an observer located at the tip of the tool fails to notice any change in the temperature distribution as the tool moves on. This assumption is generally accepted when the workpiece is long enough compared to the penetration depth of the heat transfer field.

3.3 Electrical Power

The electrical power measured directly at the input of the machine electric motor allows the determination of the input power P_{prov}. During the test, the electrical power P_R is measured in two configurations: First, when the electrical motor is unloaded, and then during turning. The mechanical power P_{prov} effectively consumed by the cutting process is the difference between these two measurements. To determine the mechanical power P_{prov} consumed by the spindle, the motor electrical efficiency coefficient η_E and the mechanical efficiency coefficient η_M of the kinematics chain have to be considered.

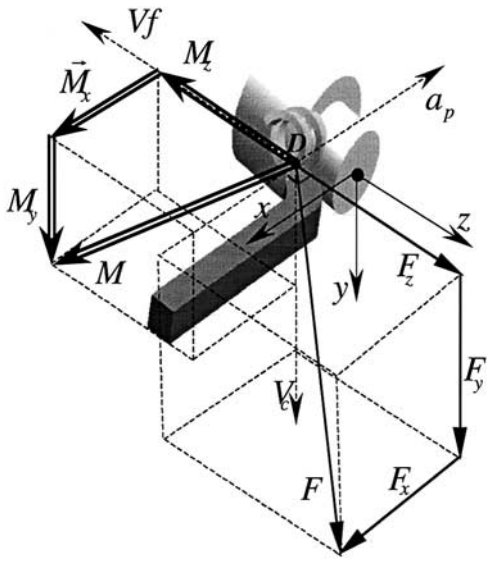

Fig. 11. Measurements of mechanical actions (forces and moments).

Experimental measurements have been carried out and a relationship makes it possible to take into account these two efficiency coefficients. Therefore, the relation between P_R and P_{prov} can be expressed by:

$$P_{prov} = f(P_R, \eta_M, \eta_E) = 1 \times 10^{-12}\, P_R^4 - 4 \times 10^{-08}\, P_R^3 + 0.0004\, P_R^2 \quad (23)$$

with a correlation coefficient $R = 0.998$.

This relation is available only for the specific lathe and test conditions used. In the two following examples, P_{mod}, P_m, P_{th}, and P_{prov} are compared.

4. Results

Initial Conditions

Two Configurations. The first set of experiments have been carried out on C38 steel with a TNMM 16 04 08 tool insert and the second on cemented steel (65 HRC hardness) with a TNMM 16 04 08 CBN tool insert. The turning parameters are summarised in Tables 1 and 2.

Table 1. Experimental and calculated parameters for the first configuration.

D_i(mm)	N (rev min^{-1})	f (mm rev^{-1})	a_p (mm)	γ (deg.)	λ (deg.)	α (deg.)
69.86	697	0.1	1	−6	24	6
V_c (ms^{-1})	V_{chip} (ms^{-1})	V_f (ms^{-1})	ρC_p (J m^3 K)	Φ (deg.)	S (mm^2)	L (mm)
2.47	1.53	0.0011	3.58×10^6	30	0.1	0.173

Table 2. Experimental and calculated parameters for the second configuration.

D_i (mm)	N (rev min^{-1})	f (mm rev^{-1})	a_p (mm)	γ (deg.)	λ (deg.)	α (deg.)
69.45	840	0.1	0.185	−6	24	6
V_c (ms^{-1})	V_{chip} (ms^{-1})	V_f (ms^{-1})	ρC_p (J m^3 K)	Φ (deg.)	S (mm^2)	L (mm)
2.89	1.79	0.0013	3.75 ± 10^6	30	0.0185	0.173

Estimated Power P_{mod}

The estimated power is given for the two configurations in Table 3. We find the three separate powers relating to the forces, moments, and kinematics parameters.

Mechanical Power P_M

Mechanical measurements have been performed during the two configurations encountered previously and are reported in Fig. 12.

The mechanical power involved by the cutting process is decomposed in Table 4. The dynamometer accuracy is about ±8 N for forces and ±0.5 Nm for moments in this loading case.

Table 3. Estimated power P_{mod} for the two configurations.

Configuration	F_yV_c (W)	F_zV_f (W)	$M_z\omega$ (W)	P_{mod} (W)
First	742	16	445	1203
Second	270	9	239	518

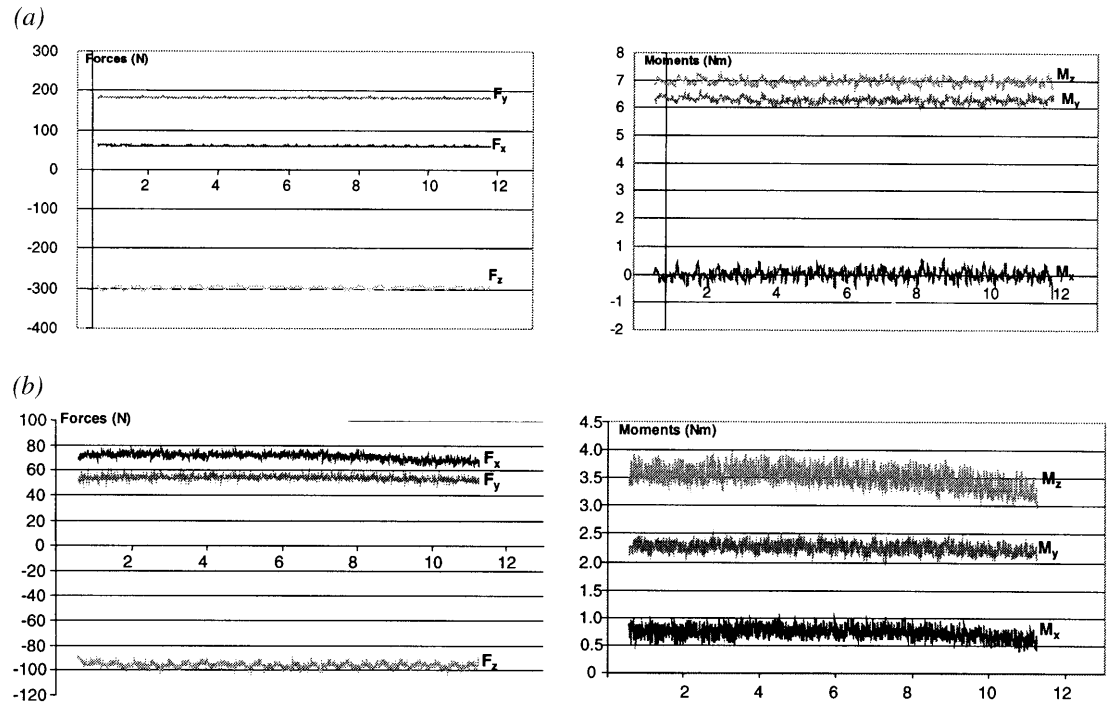

Fig. 12. Forces F_x, F_y, F_z, and moments at point D, M_x, M_y, and M_z measurements during turning of C38 steel and cemented steel. (*a*) First configuration; (*b*) second configuration.

Table 4. Mechanical power P_m decomposition for the two configurations.

Configuration	F_yV_c (W)	F_zV_f (W)	$M_z\omega$ (W)	P_m (W)
First	735 ± 20	0.21 ± 0.01	459 ± 36	1194 ± 56
Second	277.5 ± 23.5	−0.07 ± 0.01	190 ± 42	467 ± 65

Thermal Power P_{th}

First, the temperature T_c (temperature at the tip of the tool) and the heat flux ϕ_t in the tool are estimated from T_m temperature measurements during machining. These values of T_m are plotted in Fig. 13 for the two configurations of machining and the two materials. Then, T_c and ϕ_t are computed by the principle of superposition from the results of the calibration of the tool as plotted in Fig. 13 [25]. Finally, we found the total heat flux dissipated for each configuration (see Table 5).

Mechanical Provided Power P_{prov}

Mechanical input power for the two configurations is given in Table 6. Results are given in Fig. 14.

Comparison Between the Four Powers

The calculated, mechanical, thermal and mechanical input powers involved in the two machining configurations are reported in Table 7. We can see that is very good agreement between the four powers for the two configurations.

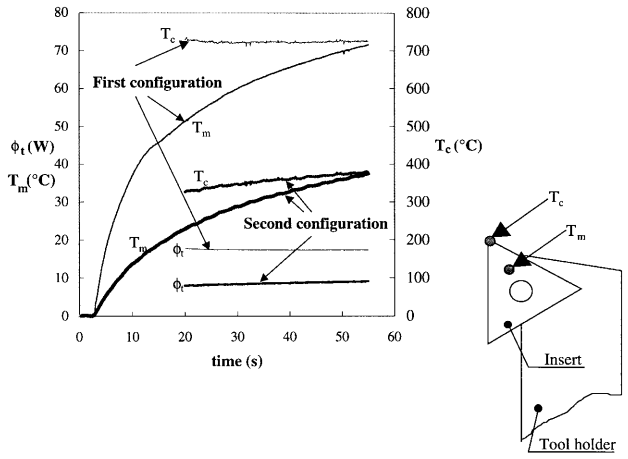

Fig. 13. T_m measurements for the two machining configurations. Estimation of T_c and ϕ_t during quasi-stationary condition.

Table 5. Thermal power P_{th} results.

First configuration$_{th1}$	Second configuration P_{th2}
$T_c = 725°C$	$T_c = 357°C$
$\phi_t = 17.4$ W	$\phi_t = 8.56$ W
$\phi_w = 294$ W	$\phi_w = 139$ W
$\phi_c = 971$ W	$\phi_c = 329$ W
$P_{th1} = \phi_t + \phi_w + \phi_c = 1283$ W	$P_{th2} = \varphi_t + \varphi_w + \varphi_c = 477$ W

Table 6. Mechanical provided power P_{prov}.

First configuration P_{prov1}	Second configuration P_{prov2}
1139 W	439 W

Table 7. Comparison between calculated, mechanical, thermal and mechanical provided powers.

First configuration				Second configuration			
P_{mod}	P_m	P_{th}	P_{prov}	P_{mod}	P_m	P_{th}	P_{prov}
1203 W	1194 W	1283 W	1139 W	518 W	467 W	477 W	439 W

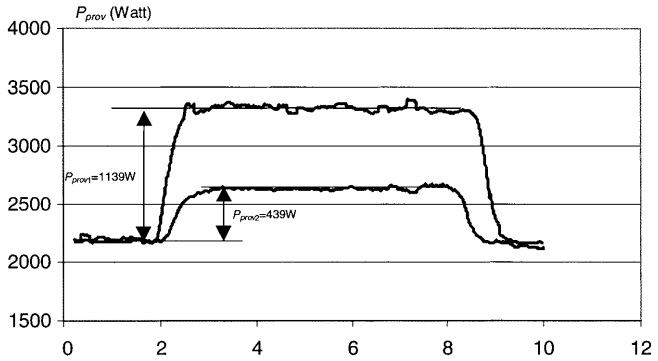

Fig. 14. Mechanical power P_{prov} in the two configurations.

1. The relative deviation between mechanical power involved at the spindle and the mechanical power consumed by the cutting process can be estimated to be from 5% to 6.5% and for the thermal power from 7.5% to 8.6%.
2. The model results are over-estimated compared to the experimental ones. A more detailed model of the secondary shearing zone is necessary. The behaviour law in this zone must be improved to take into account the real phenomena due to the stress torques and to refine the moment results.
3. Moments in all cases take a non-negligible part in the energy balance sheet. In the two cases studied, the mechanical power related to moments can be seen to be more than 40% of the total mechanical power.
4. An energy balance equilibrium is reached only if the moments are considered.

5. Conclusion

The estimated P_{mod}, mechanical P_m, thermal P_{th}, and mechanical provided P_{prov} powers involved during a 3D turning process have been determined using a model and the specific apparatus. The numerical estimated power is obtained using a new 3D model. The mechanical power is derived from the forces and moments measurements at the tip of the tool insert, since the kinematics parameters are known from the turning parameters. The thermal power is obtained from an estimation of the heat fluxes at the tool, and at the chip and the workpiece. The agreement between these three powers and the input power allows us to affirm that the cutting process produces moments at the tip of the tool. So, the contact between the tool and the workpiece cannot be considered as a point contact, but as a complete contact in 3D cutting.

For the first time, the six components of the mechanical action induced by the cutting process have been measured, and an energy balance sheet has been established with very good accuracy.

This study coupled with an operational analysis leads to a complete 3D model [13]. This model has been validated by experiments in turning and it can be generalised to drilling and milling processes.

The usual cutting models should be reconsidered to conform with the new hypothesis, especially to model the workpiece/tool contact.

References

1. P. Joyot, "Modélisation numérique et expérimentale de l'enlèvement de matière, application à la coupe orthogonale", Thèse à l'Ecde Nationale d'Ingénieurs Tarbes, France, 1994.
2. E. G. Loewen and M. C. Shaw, "On the analysis of cutting tool temperature", Transactions ASME, pp. 217–224, 1954.
3. E. Merchant, "Mechanics of the metal cutting process, orthogonal cutting and a type 2 chip", Journal of Applied Physics, 16, pp. 267–275, 1945.
4. B. T. Chao and K. J. Trigger, "Temperature distribution at tool-chip and tool–work interface in metal cutting," Transactions ASME, 56, pp. 311–320, 1956.
5. P. Gilormini, "Contribution à la modélisation de la formation du copeau en usinage des métaux", Thèse à l'Ecole Nationale Superieure Mines Paris, France, 1982.
6. P. L. B. Oxley, "Modeling machining processes with a view to their optimization and to the adaptive control of metal cutting machine tools", Robotic and Computer-Integrated Management 4, (1/2), pp. 103–119, 1988.
7. G. Boothroyd and W. A. Knigh, Fundamentals of Machining and Machine Tools, 2nd edn, Marcel Dekker, New York, 1989.
8. P. Albrecht, "New developments in the theory of metal cutting process. Part I: the ploughing process in metal cutting", Transactions ASME Journal of Engineering for Industry, 82(1), 348–358, 1960.
9. A. C. Eringen, "Linear theory of micropolar elasticity", Journal of Mathematics and Mechanics, 15 (6), pp. 909–923, 1966.
10. W. F. Hasting, P. Mathew and P. L. B. Oxley, "A machining theory for predicting chip geometry, cutting forces etc. from work material properties and cutting conditions", Proceedings of the Royal Society, London 371, pp. 569–587, 1980.
11. K. Washizu, 1968, Variational Methods in Elasticity and Plasticity, Pergamon.
12. K. L. Johnson, "Surface interaction between elastically loaded bodies under tangential forces", Proceedings of the Royal Society, London, A 230 (13), pp. 531–548, 1954.
13. D. Toulouse, "Contribution à la modélisation et à la métrologie de la coupe dans le cas d'un usinage tridimensionnel", Thèse University Bordeaux 1, France, 1998.
14. P. L. B. Oxley and M. G. Stevenson, "Measuring stress/strain properties at very high strain rates using machining test", Journal of the Institute of Metals, 95, pp. 308–313, 1967.
15. S. Kato, K. Yamgushi and M. Yamada, "Stress distribution at the interface between tool and chip in machining", Transactions AJME Journal of Engineering for Industry, pp. 683–689, 1972.
16. P. Germain, "Cours de mécanique des milieux continus", Masson & Cie, Paris, France, pp. 79–90, 1973.

17. O. Cahuc, D. Toulouse, Y. Couétard Y. and A. Gerard, "Un nouveau modèle de la zone de contact outil copeau", Comptes Rendu Academie des Sciences Paris, France, IIb 328, pp. 1–4, 2000.
18. Salençon, "Mécanique des milieux continus", Ellipse, vol. 1, Paris, France, 1988.
19. Ph. Darnis, O. Cahuc and Y. Couétard, "Energy balance with mechanical actions measurement during a turning process", Internatonal Seminar on Improving Machine Tool Performance, Nantes, France, 3–5 July 2000.
20. K. L. Johnson, "A note on the adhesion of elastic solids", British Journal of Applied Physics, 9, pp. 199–200, 1958.
21. K. L. Johnson, K. Kendall and A. D. Roberts, "Surface energy and the contac of elastic solids", Proceedings of the Royal Society, London, A 324, pp. 301–313, 1971.
22. G. Boothroyd, "Temperatures in orthogonal metal cutting," Proceedings of the Institution of Mechanical Engineers 177 (29), pp. 789–802, 1963.
23. Y. Couétard, "Capteur de forces à deux voies et application à la mesure d'un torseur de forces", Brevet français 93403025.5, 1993.
24. H. Ay and W. J. Yang, "Heat transfer and life of metal cutting tools in turning", International Journal of Heat and Mass Transfer, 41(3), pp. 613–623, 1998.
25. J. L. Battaglia, O. Cahuc, J. C. Batsale and D. Toulouse, "Métrologie des transferts thermiques dans un bec d'outil en condition d'usinage", Mécanique Industriel Materiaux France, 52(1), pp. 155–161, 1999.
26. J. V. Beck and K. J. Arnold, "Parameter estimation in engineering and science", John Wiley, 1976.
27. J. V. Beck, B. Blackwell and C. R. St. Clair, Inverse Heat Conduction, Wiley Interscience, 1985.
28. E. P. Scott and J. V. Beck, "Analysis of order of the sequential regularization solutions of inverse heat conduction problems", Journal of Heat Transfer, 111, pp. 218–224, 1989.
29. H. Stehfest, "Remarks on algorithm 368 – Numerical inversion of Laplace transforms", Communications ACM, 13, p. 624, 1970.
30. A. N. Tikhonov and V. Y. Arsenin, Solutions of Ill-Posed Problems, V. H. Winston, Washington, DC, 1977.
31. R. G. Watts, "Temperature distributions in solid and hollow cylinders due to a moving circumferential ring heat source", Journal of Heat Transfer, pp. 465–470, November 1969.

Notation

A,B	Behaviour law constants
a_p	depth of cut [mm]
D_i	workpiece diameter [mm]
C_p	specific heat [J kg^{-1} K^{-1}]
E	elasticity modulus [Pa]
F	forces vector [N]
f	feedrate [mm ref^{-1}]
h_1	primary shear zone thickness [mm]
H	constant
k	computed parameter
l	chip thickness [mm]
L,L'	clearance contact length [mm]
M	moments vector [Nm]
m	viscosity parameter
n	work hardening parameter
N	rotation frequency [rev. mn^{-1}]
p	hydrostatic pressure [Pa]
P_{mod}	estimated power [W]
P_m	mechanical power [W]
P_{prov}	provided power [W]
P_{th}	thermal power [W]
P_R	electrical power [W]
R_a	tool edge radius [mm]
S	section [m^2]
s	curvilinear coordinate
t	time [s]
T_c	calculated temperature [K]
V_c	cutting speed [ms^{-1}]
V_{chip}	chip velocity [ms^{-1}]
V_f	feed velocity [ms^{-1}]
T_m	measured temperature [K]
α	clearance angle [rd]
Φ	primary shearing angle [rd]
ϕ	heat flux [W]
θ	temperature [K]
δ	estimated coefficient
ψ	Tay constant
γ	rake angle [rd]
λ	rubbing angle [rd]
ρ	density [kg m^{-3}]
$\dot{\epsilon}$	strain
$\dot{\gamma}$	internal strain speed
σ	stress [MPa]
ω	angular velocity [rd s^{-1}]

Indices

w	workpiece
c	chip
t	tool
x, y, z	*axis components*

Operators and special functions

$\bar{}$	average
$_{int}$	interface
$\bullet$	derivative value
R	correlation function